UC San Diego

UC San Diego Previously Published Works

Title

Gain and Noise Analysis of Non-Foster Matched Antennas

Permalink

https://escholarship.org/uc/item/6p2174bv

Journal

IEEE TRANSACTIONS ON ANTENNAS AND PROPAGATION, 64(12)

ISSN

0018-926X

Authors

Jacob, Minu M
Sievenpiper, Daniel F

Publication Date

2016

DOI

10.1109/TAP.2016.2617380

Peer reviewed

eScholarship.org Powered by the California Digital Library
University of California

Gain and Noise Analysis of Non-Foster Matched Antennas

Minu M. Jacob, *Student Member, IEEE*, and Daniel F. Sievenpiper, *Fellow, IEEE*

***Abstract*— Non-Foster matching networks can overcome the gain-bandwidth limitations of passive small antennas, but at the cost of increased noise generated by the active matching circuit. Gain and noise measurements of a non-Foster matched small loop antenna were compared with those of the passive loop antenna to quantify the improvement in received signal-to-noise ratio (SNR) with non-Foster matching. The average gain improvement of 7 dB from 30–135 MHz was accompanied by an average added noise of 8.9 dB, indicating that the non-Foster matched antenna did not provide any improvement in the received SNR compared with the passive antenna. These results led to a study of the various noise sources in a non-Foster receiving system. Noise models were developed for the balanced and unbalanced Linvill negative impedance convertor circuits and verified with simulations. Simulations were then done to analyze the noise figure (NF) of a non-Foster receiving system for various small antennas, different biasing conditions, and receiver noise levels. These were then compared with NF simulations of small antennas attached to an amplifier and a noisy receiver. The results indicate that for receivers with low-noise floor levels, a receiving system consisting of a passive small antenna and an amplifier can provide better SNRs compared with a receiving system with a non-Foster matched small antenna.**

***Index Terms*— Active antenna matching, antenna noise, negative impedance convertor (NIC), non-Foster circuit (NFC), signal-to-noise ratio (SNR), small antennas.**

I. Introduction

THE demand for miniaturized, broadband communication systems has created a need for electrically small, broadband antennas. However, all passive electrically small antennas have a fundamental gain-bandwidth limitation, as first described by Wheeler [1] and Chu [2]. In recent years, active non-Foster circuits (NFCs) have been used to improve the matching bandwidth of electrically small antennas [3]–[5]. However, for an NFC matched antenna in the receiving mode, the noise added by the active NFC can degrade the received signal-to-noise ratio (SNR) beyond an acceptable limit and counteract the benefits of bandwidth improvement. While there have been a few publications on the improved matching bandwidth of NFC matched antennas, only a few publications have examined the NFC's noise performance [3], [6], but these publications present conflicting conclusions on the SNR advantage provided by non-Foster matched antennas. Furthermore, their results have not been validated with corresponding measurements and simulations that can provide an understanding of the effects of environmental noise, the receiver's noise floor, and circuit noise contributions.

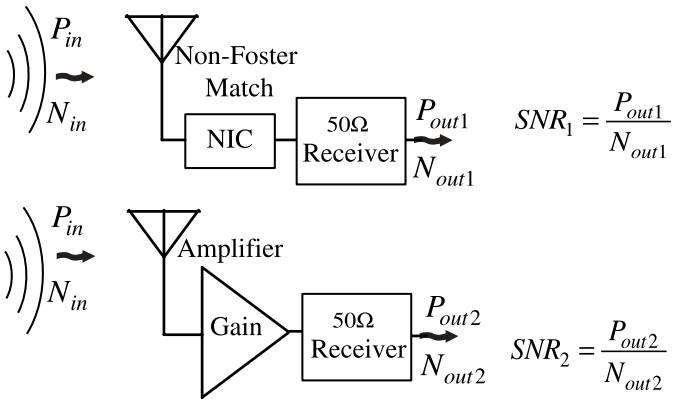

Fig. 1. Received SNR of a non-Foster matched antenna compared with that of a passive antenna attached to an amplifier.

With that objective, we designed a non-Foster matching network for a small antenna that provided a matching bandwidth from 30 to 135 MHz, performed noise simulations, and verified those simulation results with measurement results. We found that the non-Foster matched antenna did not provide a measured SNR improvement over the passive antenna, in contrast to the findings in [3]. We, therefore, undertook a detailed analysis of the various noise contributions in a non-Foster receiving system, namely, from the environment, the receiver's noise floor, and the NFC. Generalized noise models were derived for the balanced and unbalanced Linvill negative impedance convertor (NIC) circuits [7] to understand the effects of bias currents, transistors, and attached *RLC* components. The alternative to non-Foster matching is to connect the antenna directly to an amplifier, as shown in Fig. 1. To provide a fair comparison, we analyze these two cases using the same transistor technology and bias conditions for the NFC and the amplifier. This paper will present the results of noise figure (NF) comparisons for both systems, for various biasing currents, small antenna types, and most importantly, for different internal noise floor levels of the receiver, to address the question of if or under what conditions non-Foster matching can provide an advantage in small antenna receive applications.

Manuscript received June 22, 2015; revised May 8, 2016; accepted September 8, 2016. Date of publication October 13, 2016; date of current version December 5, 2016. This work was supported by the National Science Foundation under Grant 1306055.

The authors are with the University of California at San Diego, La Jolla, CA 92093 USA (e-mail: mmjacob@ucsd.edu; dsievenpiper@eng.ucsd.edu).

Color versions of one or more of the figures in this paper are available online at http://ieeexplore.ieee.org.

Digital Object Identifier 10.1109/TAP.2016.2617380

0018-926X © 2016 IEEE. Personal use is permitted, but republication/redistribution requires IEEE permission.
See http://www.ieee.org/publications_standards/publications/rights/index.html for more information.

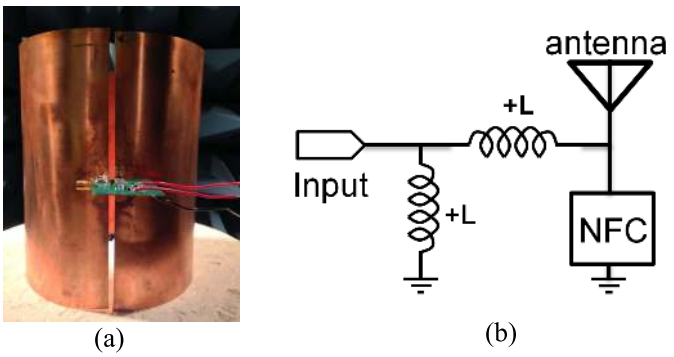

Fig. 2. (a) Loop antenna with active matching network circuit. (b) Active matching network model with the inductive transformer and NFC.

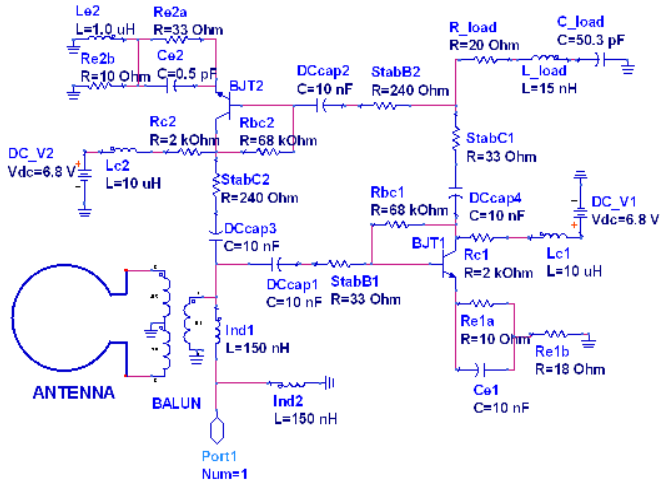

Fig. 3. NFC schematic.

II. Gain and Noise Measurements for a Non-Foster Matched Loop Antenna

A loop antenna of diameter 16 cm and height 20 cm with a resonant slot of width 3 mm was designed, as shown in Fig. 2(a). For this antenna, we designed a non-Foster matching network consisting of a −97 nH||−5.4 pF NFC, and an inductive resistance transformer, as shown in Fig. 2(b). The NFC cancels the reactance of the antenna, and the inductive transformer transforms the antenna's resistance to 50 Ω. The circuit schematic has been detailed in Fig. 3.

A. Measured Broadband Match With a Non-Foster Matching Circuit

A cosimulation technique was used wherein an electromagnetic simulation software, such as Ansys HFSS [8], was used to extract the layout parasitics and a circuit simulation software, such as Keysight ADS [9], was used to attach actual device models to the layout. The transistors used were Avago AT41511 Bipolar Junction Transistor (BJTs). The circuit was optimized to have low loss in the matching bandwidth, while providing the necessary reactance to cancel the reactance of the antenna. The NFC was designed to be stable with the inductive resistance transformer and the antenna; therefore,

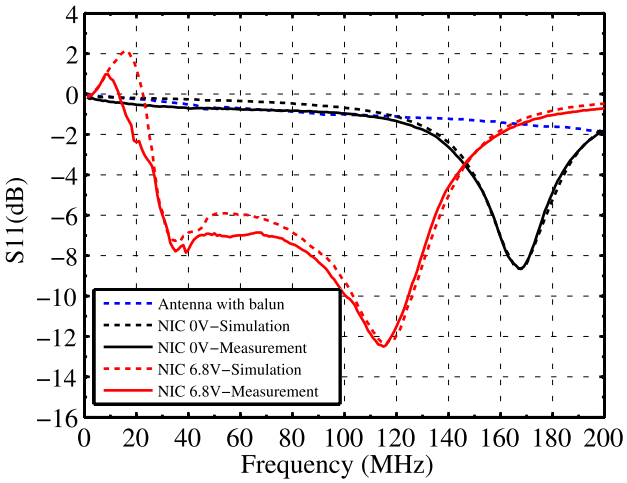

Fig. 4. $|S_{11}|$ of the passive antenna and the NFC matched antenna.

an accurate deembedded NFC measurement could not be obtained. The $-L||-C$ circuit was implemented as a short-circuit stable (SCS), single-ended configuration [7]. Since the loop antenna has a balanced mode of operation, a balun was used to convert the antenna's balanced feed to the NFC's single-ended feed. The input matching characteristics of the balun-fed antenna is shown in Fig. 4. The entire matching network consisting of the NFC and inductive transformer was fabricated on an FR-4 printed circuit board and attached to the antenna. When the NFC bias was turned OFF, the inductive resistance transformer acted as a passive matching network and provided a measured −6 dB match from 157 to 177 MHz, as shown in Fig. 4. When the NFC bias was turned ON, we achieved an improved measured −6 dB matching bandwidth from 30 to 135 MHz. In Fig. 4, it is seen that $|S_{11}|$ is greater than 1 for some low frequencies. However, the NFC was found to be stable at all frequencies. The simulated and measured input matching characteristics are very similar, as shown in Fig. 4. The measured bandwidth corresponds to a measured antenna quality factor of 0.91 computed using [10]

$$Q_{\text{meas}} = \frac{1}{\text{fractional bandwidth}}\left(\frac{\text{VSWR}-1}{\sqrt{\text{VSWR}}}\right). \tag{1}$$

The Wheeler–Chu minimum antenna quality factor corresponding to an antenna of electrical size ka = 0.28 at the matched center frequency is found to be 48.75 using [10]

$$Q_{\text{Chu}} = \frac{1}{ka} + \frac{1}{(ka)^3}. \tag{2}$$

Thus, the active matching network provides a matching bandwidth that is 53.7 times the maximum Wheeler–Chu bandwidth for an antenna of electrical size ka = 0.28.

The efficiency of a passive impedance matching network is determined by its resistive loss. For an active matching network, the efficiency should not only be determined by the loss in the circuit, but also by the noise generated by the active and passive circuit components. A perfectly lossless active matching circuit can have 100% efficiency, but can still be detrimental to a receiving antenna if it adds more noise than

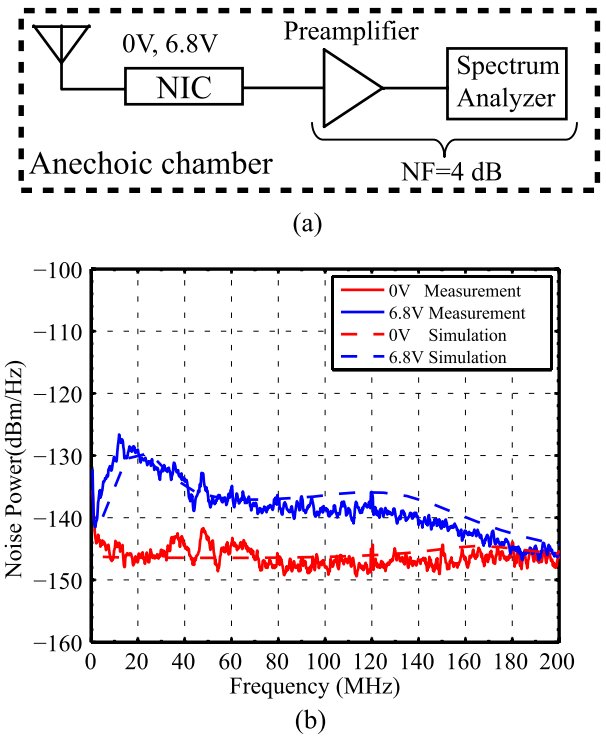

Fig. 5. (a) Measurement setup to determine noise added by the NFC. (b) Measured and simulated noise power.

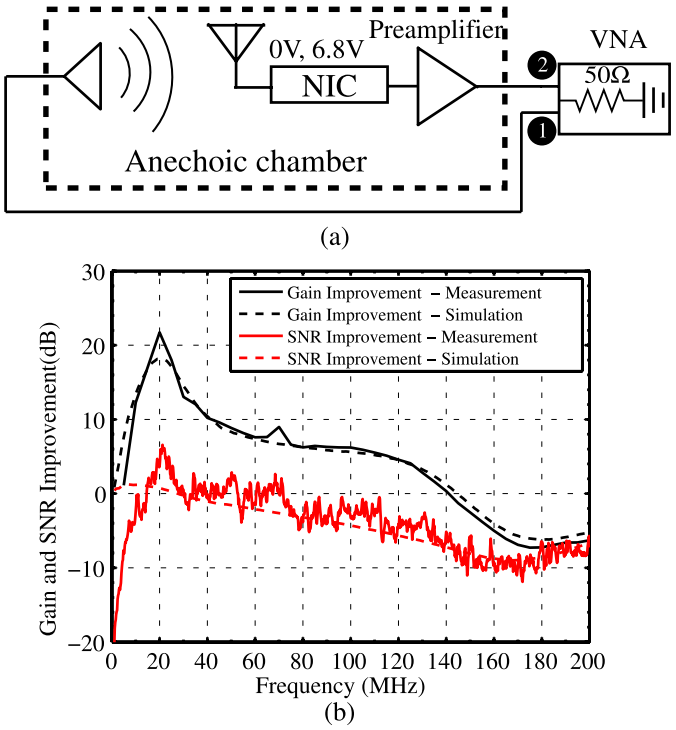

Fig. 6. (a) Measurement setup to determine gain improvement with the NFC. (b) Gain improvement compared with the SNR improvement.

the signal gain it provides. Therefore, it is important to study the noise generated by the NFC and the matching network.

B. Noise Measurements

To perform accurate noise measurements, it is important to have a receiver that has a low-NF or noise temperature (*NT*), so that small noise power levels will not be masked by the noise floor of the receiver. A Keysight EXA N9010A spectrum analyzer was used to measure the noise spectrum of our NFC matched antenna. Since the spectrum analyzer had an NF of 23 dB as calculated from its noise floor power level, we attached a low-noise preamplifier with a gain of 25 dB and an *NF* of 3 dB to the spectrum analyzer to obtain a receiver that had an low *NF* of 4 dB under matched conditions. The loop antenna with the non-Foster matching network was attached to this receiver, and the entire system was placed in an anechoic chamber, as shown in Fig. 5(a). The noise spectrum at the receiver (spectrum analyzer with preamplifier) was recorded when the NFC was turned OFF (0 V) and on (6.8 V), and the measured results are shown in Fig. 5(b). A noise simulation was also performed using ADS, where the cosimulation model of the NFC was attached to the noise models of the preamplifier and spectrum analyzer. Thermal noise from the resistive loss in the balun has also been taken into account [both in measurements and simulations in Fig. 5(b)] for the active as well as the passive antenna. We see from Fig. 5(b) that the simulated noise is similar to the measured noise, validating our noise measurements. The total noise at the receiver is a measure of the received environmental noise, the added NFC noise, and the receiver noise floor. The added noise from the NFC cannot be isolated from the total measured noise, and so it is not possible to calculate the NF of this system. However, we can calculate the improvement in received SNR with non-Foster matching relative to the passive match with a measurement of the gain improvement.

C. Gain Measurements

To assess the signal gain provided by the matching network, we set up a measurement system in the anechoic chamber, as shown in Fig. 6(a). The transmitting horn antenna was connected to port 1 of a vector network analyzer (VNA), and the NFC matched antenna with the preamplifier was attached to port 2 of the VNA. The frequency of the transmitted signal was swept from 5 to 200 MHz, and S_{21} was measured with the NFC turned OFF (0 V) and ON (6.8 V). The difference in S_{21} between the ON and OFF cases gives the gain improvement provided by the NFC over the passive match of the inductive transformer. The subtraction in S_{21} also eliminates the effects of path loss and cable loss common to both the ON and OFF cases. We see that the NFC provides a gain improvement greater than 0 dB in the low frequencies, where $|S_{11}|$ of the NFC matched antenna is greater than 1, and also in the bandwidth where the 6.8 V NFC provides better matching than the 0 V NFC [Figs. 4 and 6(b)]. The measured gain improvement is very similar to the simulated gain improvement (also calculated using the difference in S_{21} between the ON and OFF case of the NFC), as shown in Fig. 6(b). We see that in the matching bandwidth from 30 to 135 MHz, the NFC provides an average 7-dB signal improvement.

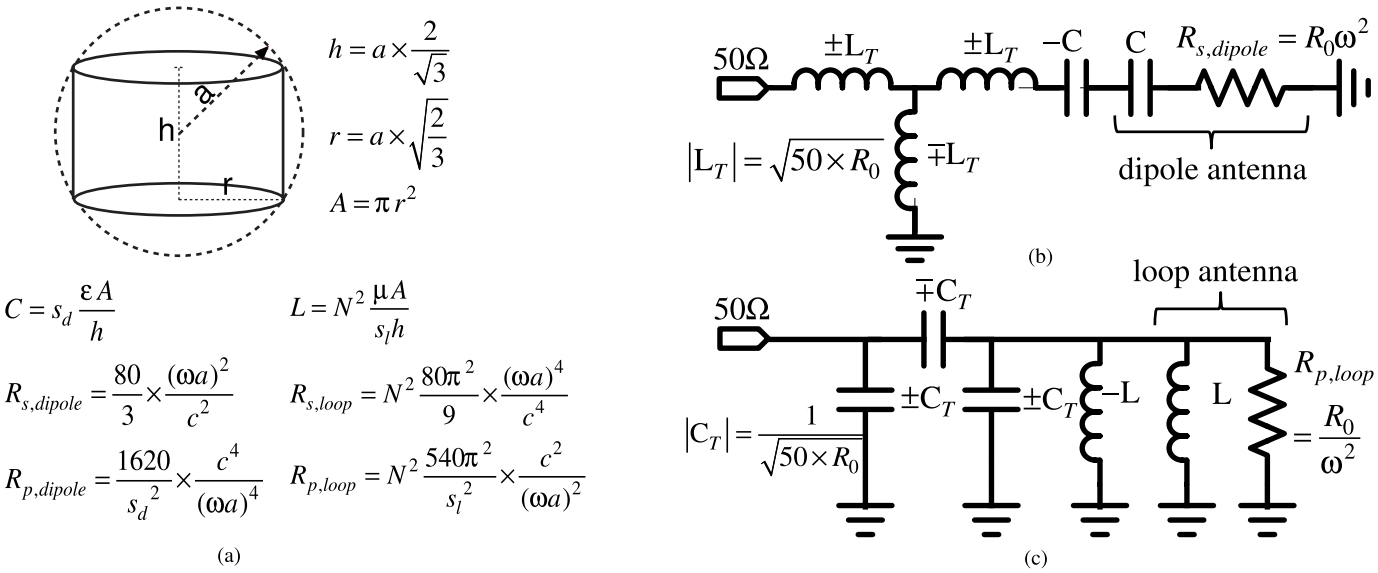

Fig. 7. (a) Wheeler's model of a capacitive small dipole antenna and an inductive small loop antenna. (b) Broadband non-Foster matching network for a small dipole antenna. (c) Broadband non-Foster matching network for a small loop antenna.

The improvement in gain is a measure of the difference in the received signal levels between the ON and OFF cases. The received noise levels have also been measured for the ON and OFF cases. The difference in the gain and noise levels has been used to calculate the improvement in received SNR between the ON and OFF cases. From the simulated and measured results in Fig. 6(b), we see that there is no improvement in the received SNR in the matching bandwidth. Thus, although the non-Foster matching network provided a broad matching bandwidth and a high signal gain improvement over a passive match, the added noise resulted in a lower received SNR compared with a passive match.

These results are contradictory to the results presented in [3], wherein measured results showed an SNR advantage with non-Foster matching. Therefore, we decided to conduct a thorough investigation of the gain and noise of non-Foster matched antennas, starting with the basis of ideal non-Foster matching for small antennas.

III. Broadband Ideal Non-Foster Match for Small Antennas

It is well known that electrically small antennas have a high quality factor Q with the minimum achievable Q being physically limited by the electrical size of the antenna ka, as seen in (2). In order to use non-Foster reactances to cancel the large reactance of the small antenna and overcome the quality factor limitation, it is helpful to calculate the reactance of a small antenna. In 1947, Wheeler [1] modeled an electrically small dipole antenna as a parallel plate capacitor and a small loop antenna as an inductive coil, both occupying a cylindrical volume of height h and a radius r. Assuming that this cylinder is circumscribed in a sphere of radius a, the height and radius of the cylinder that maximizes its volume (thus minimizing the quality factor of the small antenna) can be mathematically derived to be $h = a(2/\sqrt{3})$ and $r = a\sqrt{(2/3)}$. For a cylinder of such dimensions, the capacitance of the dipole antenna, the inductance of the loop antenna, and their respective radiation resistances and reactances can be found from [1], as shown in Fig. 7(a). Here, $R_{s,\text{dipole}}$ and $R_{s,\text{loop}}$ are the series radiation resistances of the dipole and the loop antenna. $R_{p,\text{dipole}}$ and $R_{p,\text{loop}}$ are the radiation resistances in parallel after transforming the antenna models from a series configuration to a parallel configuration. Since small antennas have a high quality factor, the reactances are approximately the same in both the series and parallel configurations, and so the capacitance of the dipole antenna and inductance of the loop antenna are the same in both configurations. s_d and s_l are the shape factors for the dipole and loop antennas, details on which can be found in [1]. Although more accurate expressions can be found for specific antenna types, the models used here are useful for identifying trends for small dipole and loop antennas.

It is apparent that even if the capacitance and inductance of the dipole and loop antennas were canceled by ideal non-Foster elements, the frequency-dependent radiation resistances of the antennas would prevent them from attaining a broadband match to a constant 50 Ω. In [11], a solution was presented in terms of a dynamic dispersive impedance transformer with complementary Foster and non-Foster inductances that can transform a radiation resistance with a squared frequency dependence into a constant resistance, in this case 50 Ω, as shown in Fig. 7(b), for a dipole antenna. However, this solution would not work for a loop antenna whose radiation resistance has a fourth power dependence on frequency. We, therefore, introduce a new scheme of a dynamic dispersive impedance transformer for a loop antenna [Fig. 7(c)]. Since loop antennas are usually matched with SCS non-Foster inductances in shunt for stability, the parallel model of the loop antenna is considered. We observe that the shunt conductance of the loop antenna has a squared frequency dependence.

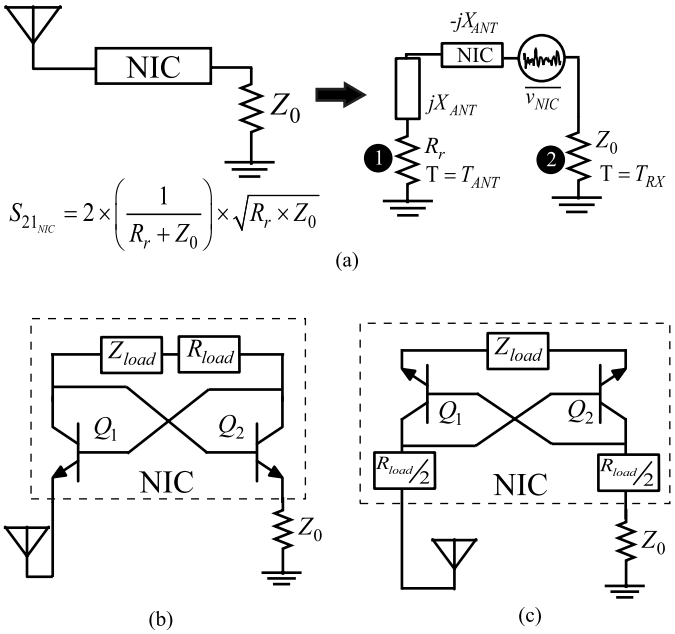

Fig. 8. (a) Floating NIC attached to a small antenna and a noisy receiver. Ideal gain shown after a lossless reactance cancellation. (b) Open-circuit stable balanced NIC for a dipole antenna. (c) SCS balanced NIC for a loop antenna.

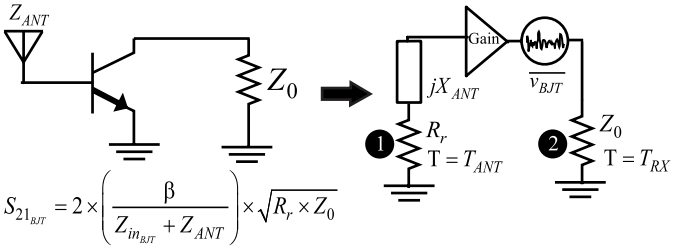

Fig. 9. Amplifier attached to a small antenna and a noisy receiver.

This leads to an impedance transformer circuit with complementary Foster and non-Foster capacitances that can transform the frequency-dependent conductance into a constant 50 Ω, as shown in Fig. 7(c). It should also be noted that both the inductive and capacitive non-Foster impedance transformers can be configured either as a π-network or a T-network.

While these ideal non-Foster matching schemes sound promising, in reality, minimizing the number of non-Foster elements is ideal for stability and simplicity, especially while analyzing noise contributions from the non-Foster circuits. Therefore, all further non-Foster matching configurations considered in this paper will assume a simple balanced Linvill NIC [7] that completely cancels the reactance of the antenna, while the radiation resistance remains frequency-dependent.

IV. System Configuration for the Noise Analysis of Non-Foster Matched and Gain-Enhanced Passive Antennas

The basic simulation setup of Fig. 1 has been extended and shown in Fig. 8 for a non-Foster matched antenna system and in Fig. 9 for a gain-enhanced unmatched antenna system.

In Fig. 8(a), the antenna has been modeled as a reactance jX_{ANT} and a radiation resistance R_r with an antenna NT T_{ANT} [12]. The values of jX_{ANT} and R_r have been calculated using the equations shown in Fig. 7(a). All loop antenna models presented in this paper assume that the number of turns $N = 2$. The antenna NT T_{ANT} has been modeled as man-made environmental noise in quiet rural areas, as reported in [13]. This frequency-dependent antenna NT has been defined in [13] using the antenna NF Fa as

$$Fa = 53.6 - 28.6 \log(f) \tag{3}$$

where f is the frequency in MHz and Fa is in units of dB(kT_0) such that $Fa = dB(T_{\mathrm{ANT}}/T_0)$ [14].

The receiver is represented as a resistance Z_0 with an NT T_{RX}, where T_{RX} is related to the noise factor F of the receiver as

$$T_{\mathrm{RX}} = (F - 1)T_0 \tag{4}$$

where T_0 is the standard NT of 290 K. The importance of including the receiver's noise floor in the system's noise analysis has been pointed out in [15]. Typically, higher frequency systems are internally noise-limited and lower-frequency systems are externally noise-limited. But if the lower-frequency systems have antennas with high mismatch or low efficiency such that the received noise power falls below the receiver's noise floor, these systems too can become internally noise-limited. It will be shown later that the noise floor of the receiver can affect the SNR advantage provided by non-Foster receiving systems, as has been previously mentioned in [5].

The NIC is modeled as a perfectly lossless reactance $-jX_{\mathrm{ANT}}$, along with an equivalent open-circuit noise voltage $\overline{v_{\mathrm{NIC}}}$ that is independent of any external loads attached to the NIC. If the NIC perfectly cancels the reactance of the antenna, then the gain of the system given by $|S_{21_{\mathrm{NIC}}}|^2$ between the radiation resistance of the antenna and the receiver is as shown in Fig. 8(a).

Fig. 8(b) and (c) shows the general non-Foster matching systems for a dipole antenna and a loop antenna, respectively. A capacitive dipole antenna typically requires an open-circuit stable (OCS) NIC for stability, whereas an inductive loop antenna requires an SCS NIC for stability. In both NIC models, Z_{load} is a reactive impedance (capacitor in the case of the OCS NIC and inductor in the case of the SCS NIC) that is negated to cancel the reactance of the antenna. An ideal balanced Linvill NIC with a finite transistor transconductance g_m has an intrinsic resistive loss (positive resistive loss in the case of the OCS NIC and negative resistive loss in the case of the SCS NIC), so a compensating R_{load} is added to both models as shown to realize a perfectly lossless balanced NIC.

Fig. 9 shows a gain-enhanced antenna receiving system, with a simple BJT amplifier providing the required gain. The bias network for the transistor has not been shown in the schematic. The BJT model used in the noise analysis is a small signal model with no noise matching or power matching. The antenna and receiver models are the same as for the non-Foster receiving systems, but the NIC of Fig. 8(a) has been replaced by a transistor along with the output-referred noise voltage of the transistor $\overline{v_{\mathrm{BJT}}}$ [16]. The gain of this system given by

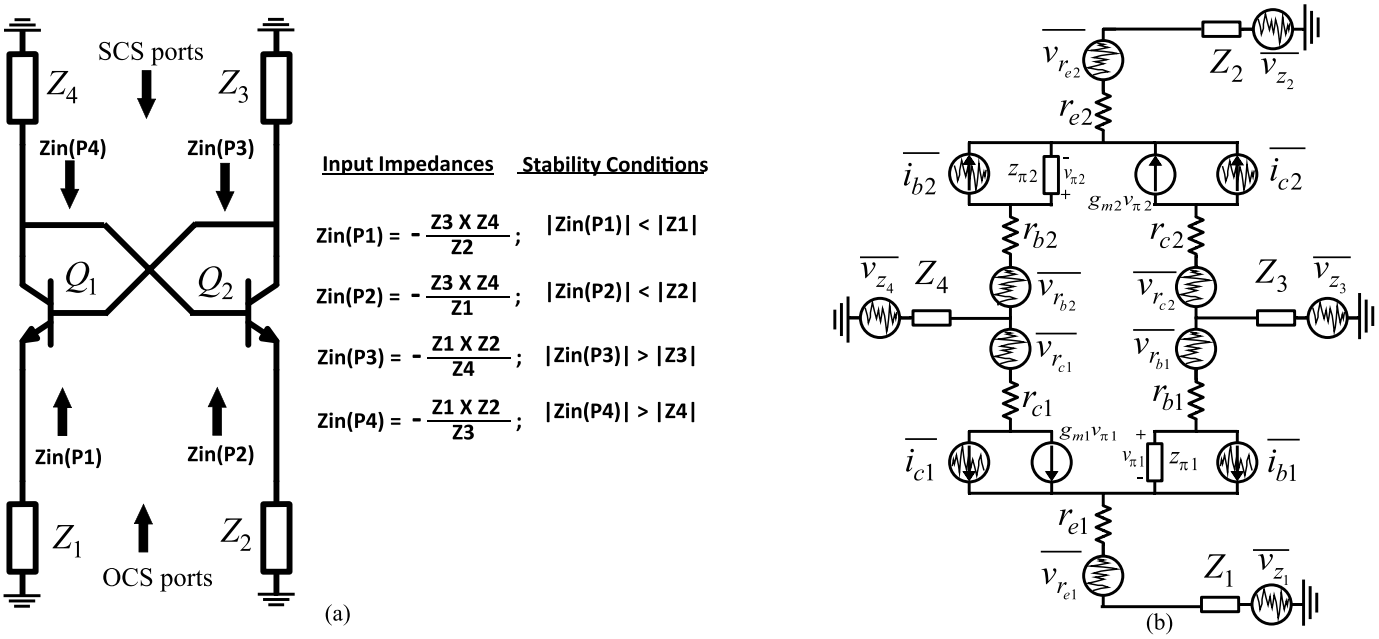

Fig. 10. (a) General topology of an NIC circuit and the input impedances seen into each of the four ports. (b) Representation of the voltage and current noise sources in a general NIC configuration.

$|S_{21_{\mathrm{BJT}}}|^2$ between the radiation resistance of the antenna and the receiver is as shown in Fig. 9, where $Z_{in_{\mathrm{BJT}}}$ is the input impedance seen looking into the transistor and β represents the current gain of the transistor.

A key difference between the non-Foster receiving system and the gain-enhanced antenna system is that the non-Foster receiving system can only have a maximum gain of 1, whereas the gain-enhanced antenna system can have a gain much greater than 1 depending on the current gain β of the transistor. Another important difference between the two systems is that the NIC is reciprocal while the amplifier is not. In the non-Foster receiving system, the internal noise of the receiver gets transmitted through the NIC and radiated out through the antenna based on the reciprocal gain $|S_{21_{\mathrm{NIC}}}|^2$ of the system. However, in the gain-enhanced passive antenna, the internal noise of the receiver sees a large impedance at the output of the amplifier and is retained at the receiver. The ramifications of these differences become apparent while analyzing overall system NFs for receivers with a high internal noise floor.

The overall system noise factor F is defined as the total noise power at the receiver divided by the transmitted input noise power. The NF is the noise factor expressed in decibels (dB)

$$NF = 10\log\left(1 + \frac{N_{\mathrm{NIC/BJT}} + N_{\mathrm{RX_{NIC/BJT}}}}{N_{\mathrm{in}} \cdot \mathrm{Gain_{NIC/BJT}}}\right) \tag{5}$$

where $N_{\mathrm{NIC/BJT}}$ is the noise power from the NIC or the BJT seen at the receiver. This can be obtained after a voltage division of $\overline{v_{\mathrm{NIC}}}$ or $\overline{v_{\mathrm{BJT}}}$ at Z_0 to obtain $\overline{v_{n,Zo}}$, and computing the noise power as $|\overline{v_{n,Zo}}|^2/Z_0$. The internal receiver noise power retained at the receiver for the NIC matched antenna or the gain-enhanced antenna is denoted as $N_{\mathrm{RX_{NIC/BJT}}}$ and can be less than the original noise floor if the system is reciprocal. The input noise power N_{in} is given by kT_{ANT}. Equations for each of these parameters will be derived in the subsequent sections.

The output noise voltage of the BJT amplifier has been previously derived [16], [17] and so we will focus on the noise model of the NIC in Section V.

V. Noise Model of the NIC

The general topology of the NIC is shown in Fig. 10(a) along with the simplified unbalanced input impedances seen looking into each of the four ports. The balanced OCS input impedance is seen looking into ports Z_1 and Z_2 and the balanced SCS input impedance is seen looking into ports Z_3 and Z_4.

Fig. 10(b) is the extended topology of Fig. 10(a), showing the small signal model of the two transistors along with the noise sources of the transistors [16] and the attached loads. The same small signal model of the transistor will be used in the gain-enhanced antenna's noise analysis, with the base of the small signal model attached to the antenna, and the collector attached to the receiver Z_0.The intrinsic base–emitter capacitor and base–collector capacitor of the transistors have been excluded for simplicity, both in the model and the subsequent simulations. All resistors, including the base resistor r_b, the collector resistor r_c, the emitter resistor r_e, and the real part of the attached loads Z_1, Z_2, Z_3, and Z_4, have a thermal noise voltage $\overline{v_{r_b}}$, $\overline{v_{r_c}}$, $\overline{v_{r_e}}$, $\overline{v_{z_1}}$, $\overline{v_{z_2}}$, $\overline{v_{z_3}}$, and $\overline{v_{z_4}}$ associated with them. These noise voltages are considered as sinusoidal generators with root-mean-square (rms) values equal to $(4kTR)^{1/2}$. The collector current and base current have corresponding shot noise currents represented as $\overline{i_c}$ and $\overline{i_b}$, with rms values equal to

$$\overline{i_c} = \sqrt{2qI_c} \tag{6}$$

$$Z_{in_{OCS,U}} \approx r_{e1} + \frac{1}{g_{m1}} - \frac{g_{m2}Z_3Z_4}{1+g_{m2}(r_{e2}+Z_2)}$$

$$\overline{v_{i_{c1,eq}}} \approx \left|\overline{i_{c1}} \times \left[Z_{in_{OCS,U}} - r_{e1} + Z_4\left(\frac{g_{m2}Z_3}{1+g_{m2}(r_{e2}+Z_2)}\right)\right]\right|$$

$$\overline{v_{i_{c2,eq}}} \approx \left|\overline{i_{c2}} \times \left[Z_2\left(\frac{g_{m2}Z_3}{1+g_{m2}(r_{e2}+Z_2)}\right) - Z_3\right]\right|$$

$$\overline{v_{i_{b1,eq}}} = \left|\overline{i_{b1}} \times \left[Z_{in_{OCS,U}} - r_{e1} - r_{b1} - Z_3\right]\right|$$

$$\overline{v_{i_{b2,eq}}} \approx \left|\overline{i_{b2}} \times \left[(Z_4 + r_{b2} + Z_2)\left(\frac{g_{m2}Z_3}{1+g_{m2}(r_{e2}+Z_2)}\right)\right]\right|,$$

where $\overline{i_c} = \sqrt{2qI_c}$ and $\overline{i_b} = \sqrt{2q\frac{I_c}{\beta}}$.

$$\overline{v_{r_{e1,eq}}} = \sqrt{4kTr_{e1}}$$

$$\overline{v_{r_{e2,eq}}} \approx \left|\sqrt{4kTr_{e2}} \times \left(\frac{g_{m2}Z_3}{1+g_{m2}(r_{e2}+Z_2)}\right)\right|$$

$$\overline{v_{r_{b1,eq}}} = \sqrt{4kTr_{b1}}$$

$$\overline{v_{r_{b2,eq}}} \approx \left|\sqrt{4kTr_{b2}} \times \left(\frac{g_{m2}Z_3}{1+g_{m2}(r_{e2}+Z_2)}\right)\right|$$

$$\overline{v_{z_{2,eq}}} \approx \left|\sqrt{4kT*real(Z_2)} \times \left(\frac{g_{m2}Z_3}{1+g_{m2}(r_{e2}+Z_2)}\right)\right|$$

$$\overline{v_{z_{3,eq}}} = \sqrt{4kT*real(Z_3)}$$

$$\overline{v_{z_{4,eq}}} \approx \left|\sqrt{4kT*real(Z_4)} \times \left(\frac{g_{m2}Z_3}{1+g_{m2}(r_{e2}+Z_2)}\right)\right|$$

(a)

$$Z_{in_{SCS,U}} \approx -\frac{(1+g_{m1}(Z_1+r_{e1}))(1+g_{m2}(Z_2+r_{e2}))}{g_{m1}g_{m2}Z_3}$$

$$\overline{v_{i_{c1,eq}}} \approx \left|\overline{i_{c1}} \times \left[Z_{in_{SCS,U}} + (Z_1+r_{e1})\left(\frac{1+g_{m2}(Z_2+r_{e2})}{g_{m2}Z_3}\right)\right]\right|$$

$$\overline{v_{i_{c2,eq}}} \approx \left|\overline{i_{c2}} \times \left[Z_3\left(\frac{1+g_{m2}(Z_2+r_{e2})}{g_{m2}Z_3}\right) - (Z_2+r_{e2})\right]\right|$$

$$\overline{v_{i_{b1,eq}}} \approx \left|\overline{i_{b1}} \times \left[(Z_3+r_{b1}+Z_1+r_{e1})\left(\frac{1+g_{m2}(Z_2+r_{e2})}{g_{m2}Z_3}\right)\right]\right|$$

$$\overline{v_{i_{b2,eq}}} = \left|\overline{i_{b2}} \times \left[Z_{in_{SCS,U}} - (Z_2+r_{e2}) - r_{b2}\right]\right|,$$

where $\overline{i_c} = \sqrt{2qI_c}$ and $\overline{i_b} = \sqrt{2q\frac{I_c}{\beta}}$.

$$\overline{v_{r_{e1,eq}}} \approx \left|\sqrt{4kTr_{e1}} \times \left(\frac{1+g_{m2}(Z_2+r_{e2})}{g_{m2}Z_3}\right)\right|$$

$$\overline{v_{r_{e2,eq}}} = \sqrt{4kTr_{e2}}$$

$$\overline{v_{r_{b1,eq}}} \approx \left|\sqrt{4kTr_{b1}} \times \left(\frac{1+g_{m2}(Z_2+r_{e2})}{g_{m2}Z_3}\right)\right|$$

$$\overline{v_{r_{b2,eq}}} = \sqrt{4kTr_{b2}}$$

$$\overline{v_{z_{1,eq}}} \approx \left|\sqrt{4kT*real(Z_1)} \times \left(\frac{1+g_{m2}(Z_2+r_{e2})}{g_{m2}Z_3}\right)\right|$$

$$\overline{v_{z_{2,eq}}} = \sqrt{4kT*real(Z_2)}$$

$$\overline{v_{z_{3,eq}}} \approx \left|\sqrt{4kT*real(Z_3)} \times \left(\frac{1+g_{m2}(Z_2+r_{e2})}{g_{m2}Z_3}\right)\right|$$

(b)

$$Z_{in_{OCS,B}} \approx r_{e1} + r_{e2} + \frac{1}{g_{m1}} + \frac{1}{g_{m2}} - Z_{load} - R_{load}$$

$$\overline{v_{i_{c,eq}}} = \left|\overline{i_c} \times \left[\frac{Z_{load}}{2} + \frac{Z_{in_{OCS,B}}}{2} - r_e + \frac{R_{load}}{2}\right]\right|$$

$$\overline{v_{i_{b,eq}}} = \left|\overline{i_b} \times \left[\frac{Z_{load}}{2} - \frac{Z_{in_{OCS,B}}}{2} + r_e + r_b + \frac{R_{load}}{2}\right]\right|,$$

where $\overline{i_c} = \sqrt{2qI_c}$ and $\overline{i_b} = \sqrt{2q\frac{I_c}{\beta}}$.

$$\overline{v_{r_{e,eq}}} = \sqrt{4kTr_e}$$

$$\overline{v_{r_{b,eq}}} = \sqrt{4kTr_b}$$

$$\overline{v_{R_{load,eq}}} = \sqrt{4kTR_{load}}$$

(c)

$$Z_{in_{SCS,B}} \approx -r_{e1} - r_{e2} - \frac{1}{g_{m1}} - \frac{1}{g_{m2}} - Z_{load} + R_{load}$$

$$\overline{v_{i_{c,eq}}} = \left|\overline{i_c} \times \left[\frac{Z_{load}}{2} + \frac{Z_{in_{SCS,B}}}{2} + r_e - \frac{R_{load}}{2}\right]\right|$$

$$\overline{v_{i_{b,eq}}} = \left|\overline{i_b} \times \left[\frac{Z_{load}}{2} - \frac{Z_{in_{SCS,B}}}{2} + r_e + r_b + \frac{R_{load}}{2}\right]\right|,$$

where $\overline{i_c} = \sqrt{2qI_c}$ and $\overline{i_b} = \sqrt{2q\frac{I_c}{\beta}}$.

$$\overline{v_{r_{e,eq}}} = \sqrt{4kTr_e}$$

$$\overline{v_{r_{b,eq}}} = \sqrt{4kTr_b}$$

$$\overline{v_{R_{load,eq}}} = \sqrt{4kTR_{load}}$$

(d)

$$\overline{v_{NIC_{OCS,U}}} = \sqrt{\left|\overline{v_{i_{c1,eq}}}\right|^2 + \left|\overline{v_{i_{c2,eq}}}\right|^2 + \left|\overline{v_{i_{b1,eq}}}\right|^2 + \left|\overline{v_{i_{b2,eq}}}\right|^2 + \left|\overline{v_{r_{e1,eq}}}\right|^2 + \left|\overline{v_{r_{e2,eq}}}\right|^2 + \left|\overline{v_{r_{b1,eq}}}\right|^2 + \left|\overline{v_{r_{b2,eq}}}\right|^2 + \left|\overline{v_{z_{2,eq}}}\right|^2 + \left|\overline{v_{z_{3,eq}}}\right|^2 + \left|\overline{v_{z_{4,eq}}}\right|^2}$$

$$\overline{v_{NIC_{SCS,U}}} = \sqrt{\left|\overline{v_{i_{c1,eq}}}\right|^2 + \left|\overline{v_{i_{c2,eq}}}\right|^2 + \left|\overline{v_{i_{b1,eq}}}\right|^2 + \left|\overline{v_{i_{b2,eq}}}\right|^2 + \left|\overline{v_{r_{e1,eq}}}\right|^2 + \left|\overline{v_{r_{e2,eq}}}\right|^2 + \left|\overline{v_{r_{b1,eq}}}\right|^2 + \left|\overline{v_{r_{b2,eq}}}\right|^2 + \left|\overline{v_{z_{1,eq}}}\right|^2 + \left|\overline{v_{z_{2,eq}}}\right|^2 + \left|\overline{v_{z_{3,eq}}}\right|^2}$$

$$\overline{v_{NIC_B}} = \sqrt{2\left|\overline{v_{i_{c,eq}}}\right|^2 + 2\left|\overline{v_{i_{b,eq}}}\right|^2 + 2\left|\overline{v_{r_{e,eq}}}\right|^2 + 2\left|\overline{v_{r_{b,eq}}}\right|^2 + \left|\overline{v_{R_{load,eq}}}\right|^2}$$

(e)

Fig. 11. (a) Input-referred equivalent noise sources for an unbalanced, OCS NIC. (b) Input-referred equivalent noise sources for an unbalanced, SCS NIC. (c) Input-referred equivalent noise sources for a balanced, OCS NIC. (d) Input-referred equivalent noise sources for a balanced, SCS NIC. (e) Total input-referred equivalent noise voltage for the unbalanced and balanced NICs.

and

$$\overline{i_b} = \sqrt{2q\frac{I_c}{\beta}} \tag{7}$$

where I_c is the collector bias current and β is the current gain $((I_c)/(I_b))$. Burst noise and flicker noise in the base current have been omitted for simplicity.

This general circuit model is used to derive the equivalent open-circuit noise voltage $\overline{v_{\mathrm{NIC}}}$ for four different configurations, namely, an unbalanced OCS NIC looking into Z_1 [Fig. 11(a)], an unbalanced SCS NIC looking into Z_4 [Fig. 11(b)], a balanced OCS NIC looking into Z_1–Z_2 [Fig. 11(c)], and a balanced SCS NIC looking into Z_3–Z_4 [Fig. 11(d)]. More information on the four different topologies can be found in [3] and [7]. For each of these configurations, the input of the NIC is left as an open and the individual noise sources are referred to the input. Each internal noise source is considered in turn, and standard sinusoidal circuit

analysis calculations are used to transform each noise source to a corresponding equivalent open-circuit noise voltage at the input. The equivalent noise transformations are shown in Fig. 11 for all four configurations of the Linvill NIC. For instance, in Fig. 11(a), $Z_{\text{in}_{\text{OCS},U}}$ is the input impedance of the unbalanced, OCS NIC configuration seen looking into Z_1. The noise voltage $\overline{v_{i_{c1,\text{eq}}}}$ is the equivalent open-circuit noise voltage at the input due to the noise source $\overline{i_{c1}}$ from the collector current of transistor $Q1$ in Fig. 10(b). It is interesting to note that $\overline{v_{i_{c1,\text{eq}}}}$ is a function of the input impedance $Z_{\text{in}_{\text{OCS},U}}$. Similar equations have been derived for all internal noise sources. For ease of representation, the equations shown are approximations assuming a large $z_{\pi 1}$ and $z_{\pi 2}$ in Fig. 10(b). The thermal noise voltage associated with the collector resistor has a negligible effect, since it is in series with a high collector impedance. Since all the individual noise sources are independent, the total noise voltage $\overline{v_{\text{NIC}}}$ at the input is the square root of the sum of the individual input-referred mean-square noise voltages, as shown in Fig. 11(e). For the balanced NIC models, the input-referred noise voltages are identical for the two transistors, leading to a factor of 2 for the mean-square noise voltages within the equation for $\overline{v_{\text{NIC}_B}}$. Thus, the equations in Fig. 11(e) represent the total open-circuit equivalent noise voltage $\overline{v_{\text{NIC}}}$ in Fig. 8(a).

An interesting result of this analysis is the discovery that the total equivalent noise of the NIC is proportional to the magnitude of the input impedance of the NIC for all four configurations of the NIC. This becomes apparent after simplifying the equations in Fig. 11 assuming a very large transconductance g_m, and a near-zero emitter resistance and base resistance. It will be seen that in such ideal conditions, the majority of noise comes from the base current's shot noise. To illustrate this for the balanced, OCS NIC in Fig. 11(c), approximations of infinite transconductance and near-zero emitter resistance and base resistance(which eliminates the need for loss compensation using R_{load}) are used to simplify the equations. This results in the input impedance $Z_{\text{in}_{\text{OCS},B}}$ being equal to $-Z_{\text{load}}$. Using this result, we see that $\overline{v_{i_{c,\text{eq}}}}$ goes to 0. The only nonzero equivalent noise voltage in Fig. 11(c) is $\overline{v_{i_{b,\text{eq}}}} = |i_b \times Z_{\text{load}}|$. Thus, we see that the total equivalent noise is proportional to the impedance of the NIC. A similar analysis can be done for all four models of the NIC in Fig. 11. Furthermore, with the knowledge of these equations, we can choose a combination of external loads Z_1, Z_2, Z_3, and Z_4 that will yield the minimum noise for a specific required non-Foster impedance. For instance, if an SCS unbalanced $-L$ was required looking into port Z_4, a configuration with Z_2 as an inductor and Z_1 and Z_3 as resistors would yield the minimum noise as opposed to inverting a capacitor at Z_3.

Noise simulations were done in Keysight ADS using the die model of the Avago transistor AT41511, but with the internal capacitors set to zero. The same transistor model was used to mathematically calculate the equivalent noise $\overline{v_{\text{NIC}}}$ using the complete form of the equations in Fig. 11(e) (including correct values of $z_{\pi 1}$ and $z_{\pi 2}$). An exact match was obtained between the simulated and calculated results, as shown in Fig. 12, for a balanced OCS negative capacitor and a balanced SCS negative inductor. A bias current of 0.5 mA was set for all the transistors, and required values of R_{load} were set to compensate for the intrinsic loss of the NIC. The values of $-C$ and $-L$ were chosen to cancel the reactance of a small dipole and a small loop that fit within a sphere of radius $a = 10$ cm, as shown in Fig. 7(a). We can further see from the calculated equivalent noise voltages that the noise voltage of the $-C$ and $-L$ NIC have the same frequency dependence as the magnitude of their respective non-Foster impedances. The unbalanced noise model's equations were also verified with simulations and found to be an exact match. After verifying the noise models, we proceeded to NF simulations of the non-Foster matched and gain-enhanced passive antennas.

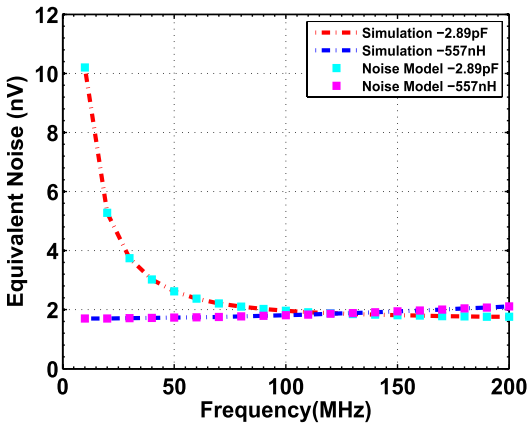

Fig. 12. Simulated and calculated total input-referred equivalent noise for a balanced OCS negative capacitor and a balanced SCS negative inductor.

VI. Noise Figure of Non-Foster Matched and Gain-Enhanced Small Antennas

NF simulations were done using the simulation setup in Fig. 8(b) for a non-Foster matched small dipole antenna and the setup in Fig. 8(c) for a non-Foster matched small loop antenna. The setup in Fig. 9 was used to simulate the NF of a gain-enhanced dipole antenna as well as a gain-enhanced loop antenna. The simulated NF corresponds to the calculation in (5). The parameters in (5) can be further expanded as shown in the following:

$$N_{\text{NIC}} = \left|\overline{v_{\text{NIC}}} \times \frac{Z_0}{Z_0 + Z_{\text{in}_{\text{NIC}}} + Z_{\text{ANT}}}\right|^2 \times \frac{1}{Z_0} \tag{8}$$

$$N_{\text{BJT}} = \left|\overline{v_{\text{BJT}}} \times \frac{Z_0}{Z_0 + Z_{\text{out}_{\text{BJT}}}}\right|^2 \times \frac{1}{Z_0} \tag{9}$$

$$N_{\text{RX}_{\text{NIC}}} = \left|2\sqrt{kT_{\text{RX}}Z_0} \cdot \frac{Z_{\text{in}_{\text{NIC}}} + Z_{\text{ANT}}}{Z_0 + Z_{\text{in}_{\text{NIC}}} + Z_{\text{ANT}}}\right|^2 \times \frac{1}{Z_0} \tag{10}$$

$$N_{\text{RX}_{\text{BJT}}} = \left|2\sqrt{kT_{\text{RX}}Z_0} \times \frac{Z_{\text{out}_{\text{BJT}}}}{Z_0 + Z_{\text{out}_{\text{BJT}}}}\right|^2 \times \frac{1}{Z_0} \tag{11}$$

$$N_{\text{in}} \cdot \text{Gain}_{\text{NIC/BJT}} = kT_{\text{ANT}} \times |S21_{\text{NIC/BJT}}|^2. \tag{12}$$

In (8)–(12), N_{NIC} and N_{BJT} correspond to noise from the NIC and the BJT, respectively, delivered to the receiver of impedance Z_0. $Z_{\text{in}_{\text{NIC}}}$ is the input impedance of the NIC given

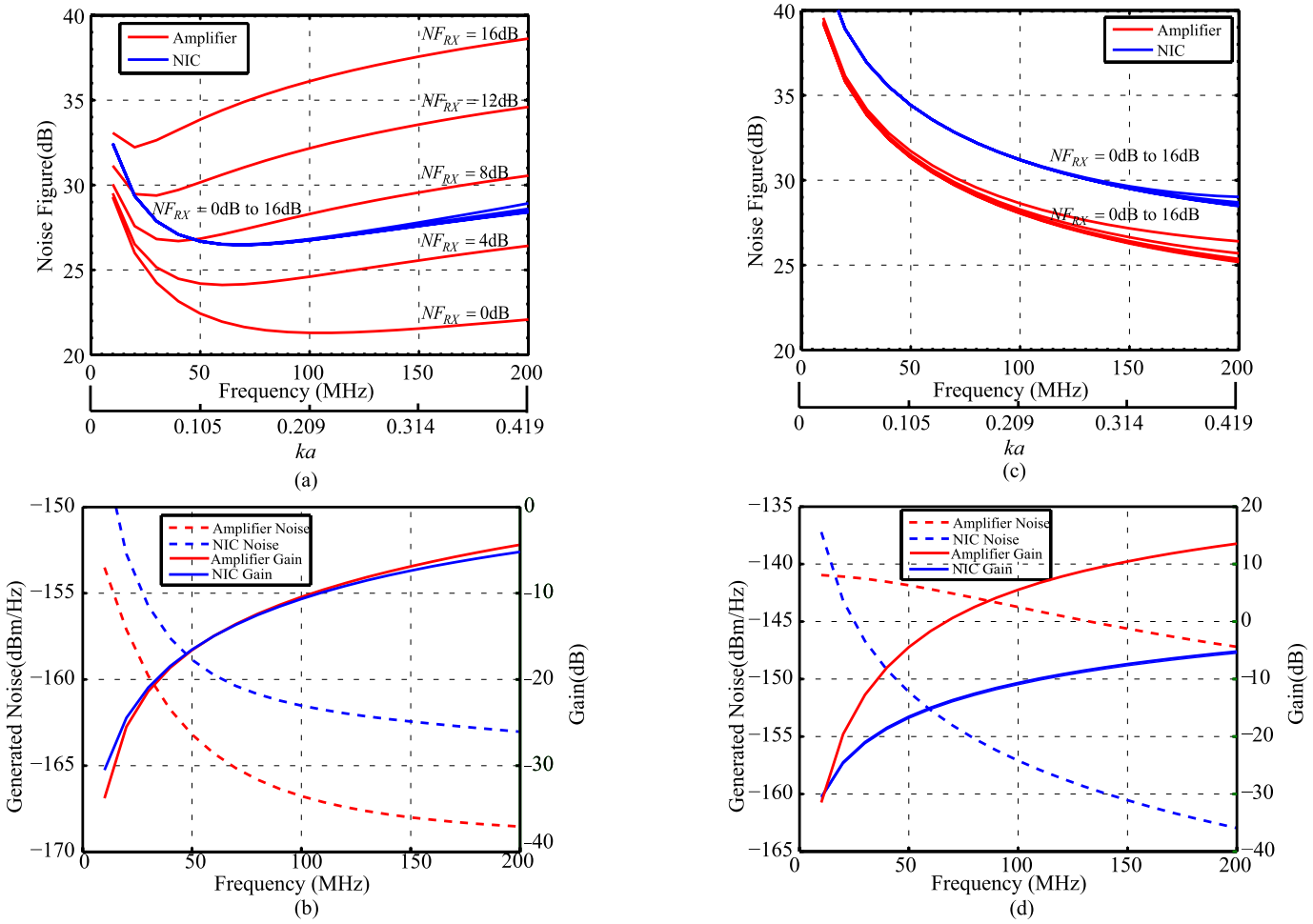

Fig. 13. (a) NF comparison between a non-Foster matched and gain-enhanced dipole antenna for different noisy receivers, where all transistors are biased at 0.5 mA. (b) Noise generated by the $-C$ NIC and the amplifier at the 50-Ω receiver, and the net gain comparison for both systems, where all transistors are biased at 0.5 mA. (c) NF comparison between a non-Foster matched and gain-enhanced dipole antenna for different noisy receivers, where all transistors are biased at 5 mA. (d) Noise generated by the $-C$ NIC and the amplifier at the 50-Ω receiver, and the net gain comparison for both systems, where all transistors are biased at 5 mA.

by the equations in Fig. 11 and Z_{ANT} is the impedance of the antenna, given by the equations in Fig. 7(a). $Z_{\mathrm{out_{BJT}}}$ is the impedance seen looking from the receiver into the output of the amplifier in Fig. 9. T_{RX} and T_{ANT} are NTs of the receiver and the antenna as defined in the previous sections. These equations are helpful in analyzing the results that are presented in Sections VI-A–VI-C.

A. Noise Figure Comparison for a Small Dipole Antenna

First, a small dipole antenna was assumed to fit within a sphere of radius $a = 10$ cm, as shown in Fig. 7(a), and the relevant antenna parameters were calculated. The same dipole was attached to an NIC and the input of a BJT, as shown in Figs. 8(b) and 9, respectively. All transistors were biased with a collector current of $I_c = 0.5$ mA and the required R_{load} was added to the NIC to realize a lossless NIC. In both systems, the receiver's NF was swept from 0 dB (ideal noiseless receiver) to 16 dB and the overall system NF was simulated, as shown in Fig. 13(a). The added noise from the NIC and the BJT as seen at the receiver ($N_{\mathrm{NIC/BJT}}$) has been plotted in Fig. 13(b) along with the net gain of both systems. Fig. 13(a) shows that the NF of the non-Foster matched small dipole antenna is largely independent of the swept receiver noise levels, unlike the gain-enhanced antenna system. This is because the internal noise of the receiver gets radiated back out through the antenna in the reciprocal non-Foster system, leading to a receiver noise level $N_{\mathrm{RX_{NIC}}}$ in (5) that is about 20 dB less than the noise level $N_{\mathrm{RX_{BJT}}}$ of the gain-enhanced antenna system, as verified through (10) and (11). Therefore, the effect of N_{RX} in (5) can be neglected for the non-Foster matched antenna system. It is thus seen that for receivers with NFs below 6 dB, the non-Foster matched antenna has a higher overall system NF compared with the gain-enhanced antenna system. It is only when the receiver is noisy with NFs above 6 dB that the non-Foster matched antenna provides a received SNR advantage compared with the gain-enhanced passive antenna.

The simulations have been repeated for a transistor bias current of 5 mA for all transistors, and the results have been plotted in Fig. 13(c) and (d). For such a large bias current, both the NIC and the BJT generate higher noise power levels, as shown in Fig. 13(d). Furthermore, the noise generated by the BJT overpowers the internal noise of the receiver, leading to

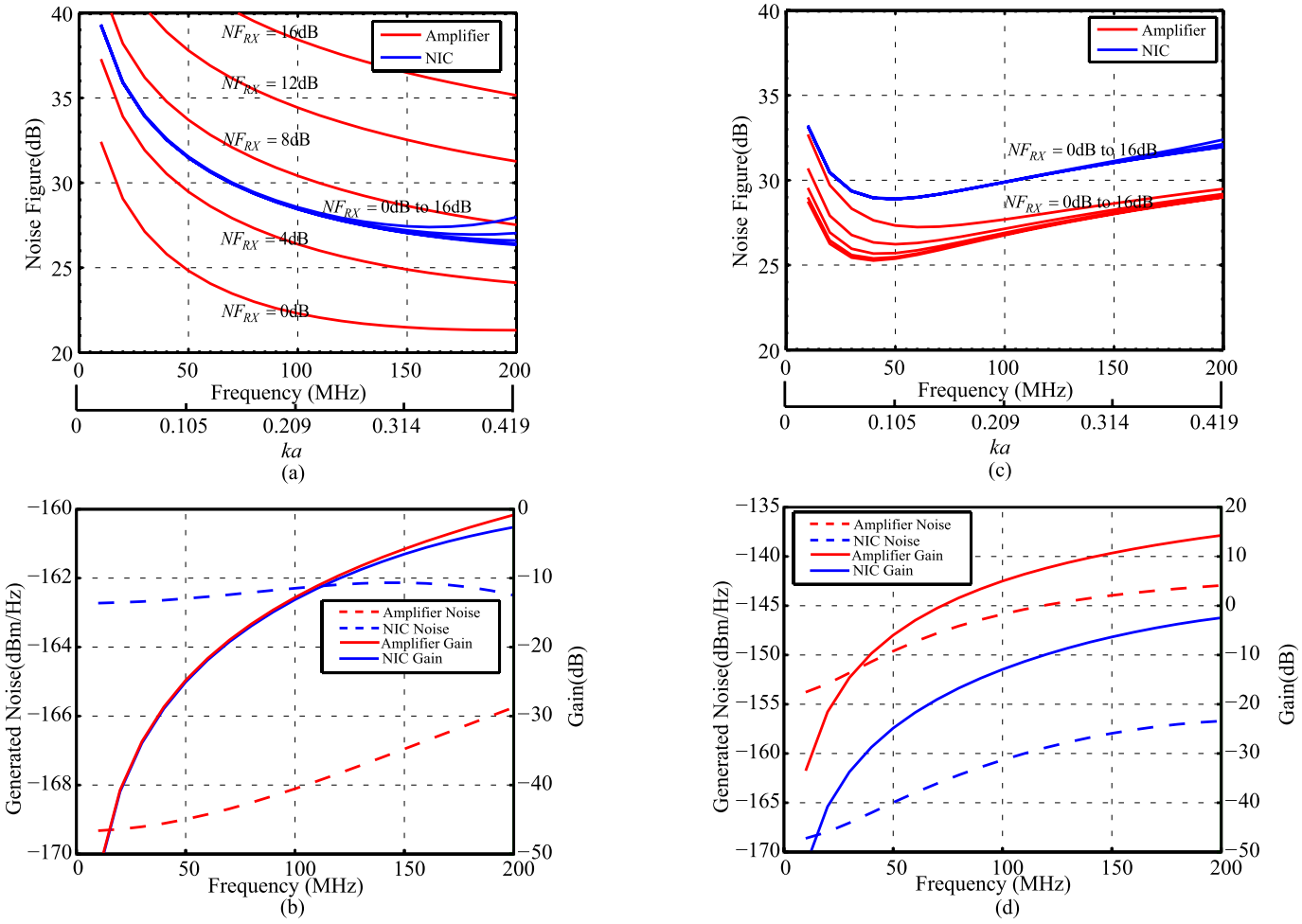

Fig. 14. (a) NF comparison between a non-Foster matched and gain-enhanced loop antenna for different noisy receivers, where all transistors are biased at 0.5 mA. (b) Noise generated by the $-L$ NIC and the amplifier at the 50-Ω receiver, and the net gain comparison for both systems, where all transistors are biased at 0.5 mA. (c) NF comparison between a non-Foster matched and gain-enhanced loop antenna for different noisy receivers, where all transistors are biased at 5 mA. (d) Noise generated by the $-L$ NIC and the amplifier at the 50-Ω receiver, and the net gain comparison for both systems, where all transistors are biased at 5 mA.

an overall system NF that is fairly independent of the internal noise of the receiver. For the non-Foster matched antenna, the internal noise of the receiver gets radiated away as before, and the overall system NF is again independent of the noise floor of the receiver. The most important difference between the two biasing conditions is in the gain of the two systems. The BJT provides a much larger gain than the non-Foster matched antenna, leading to overall lower system NFs for all considered receivers.

Thus, if there are constraints on the dc power consumption, the non-Foster matched antenna could provide an SNR advantage over the gain-enhanced antenna, but only for noisy receivers with a fairly high noise floor. If there are no constraints on the dc power consumption, it is possible to increase the gain of the amplifier to a level that provides an SNR advantage over non-Foster matched antennas for all practical receivers.

B. Noise Figure Comparison for a Small Loop Antenna

The NF simulations were repeated for a small loop antenna that was assumed to fit within a sphere of radius $a = 10$ cm. Similar results were obtained as for the small dipole antenna in Fig. 14. It is again interesting to note that for a bias condition of $I_c = 0.5$ mA for all transistors, the non-Foster matching system is better than the gain-enhanced passive system only for receivers of NF 6 dB and above. Under a bias condition of $I_c = 5$ mA, the gain-enhanced loop antenna is better than the non-Foster matched loop antenna for all considered receivers.

It is also important to note that even if we were to force the power consumption to be the same in both the non-Foster system and the gain-enhanced system by supplying twice the bias current of the NIC's transistors to the BJT, the gain-enhanced system would still provide an SNR advantage over the non-Foster receiving system for practical, low-noise receivers.

C. Noise Figure Versus Antenna Size

The results obtained for the dipole antenna and loop antenna raise questions as to the validity of those conclusions for different small antenna sizes. Therefore, we repeated the simulations for different small antennas assumed to fit within spheres of radius 10, 20, 30, 40, and 50 cm, ranging in electrical size from $ka = 0.2095$ to $ka = 1.0472$ at 100 MHz.

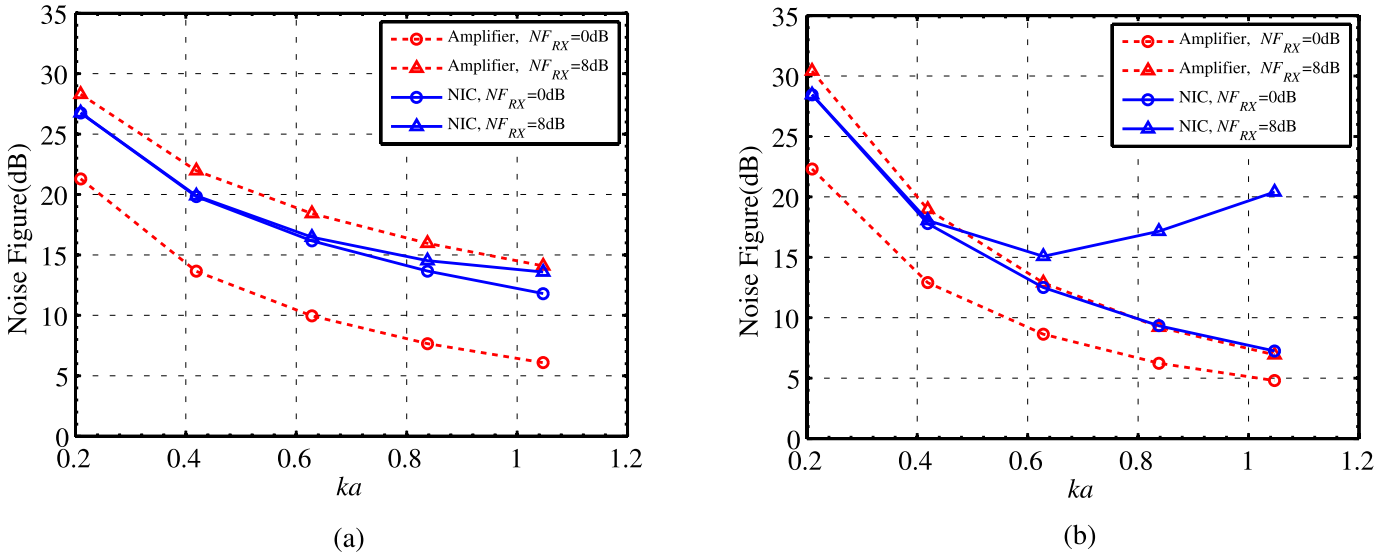

Fig. 15. (a) NF comparison between a non-Foster matched and gain-enhanced dipole antenna at 100 MHz for different antenna sizes. (b) NF comparison between a non-Foster matched and gain-enhanced loop antenna at 100 MHz for different antenna sizes.

The overall system NF values at 100 MHz for the non-Foster matched antenna system and the gain-enhanced antenna system have been plotted against the electrical size of the antenna in Fig. 15. The simulations have been done for two receivers, the first being an ideal noiseless receiver with an NF of 0 dB, and the second being a receiver of NF 8 dB. It is seen that with a perfect noiseless receiver, the non-Foster matched antenna has a higher overall system NF compared with the gain-enhanced antenna, for both the dipole and loop antennas. With the receiver of NF 8 dB, it can be seen from Fig. 15(a) that the non-Foster matched dipole antenna has a slightly lower NF than the gain-enhanced dipole antenna until the antenna's electrical size approaches 1, at which point the non-Foster matched dipole antenna starts losing its advantage. The corresponding results for the small loop antenna system have been presented in Fig. 15(b). Since the loop antenna has a radiation resistance that is proportional to the fourth power of frequency, its radiation resistance becomes significant for electrical sizes greater than 0.5. Furthermore, the inductance of the loop antenna also becomes quite large considering a two-turn loop, and the required non-Foster inductance and the corresponding generated noise also become substantial for $ka > 0.5$. Therefore, with the receiver of NF 8 dB, the overall NF of the non-Foster matched small loop antenna is lower than that of the gain-enhanced loop antenna only for $ka < 0.5$.

Thus, the conclusion that non-Foster matched antennas do not provide an SNR advantage over gain-enhanced small antennas for low-noise receivers with an NF below say, 6 dB, has been shown to be true for various small antenna sizes.

VII. Conclusion

The noise analysis and simulations presented in this paper provide explanations as to why our gain and noise measurements indicate no SNR advantage over the passive antenna, whereas measurements in [3] indicate otherwise. The measurements in [3] have been done using a receiver of NF 8 dB, whereas the measurements presented in this paper have been done with a receiver of NF 4 dB. Furthermore, it has been conceded in [3] that non-Foster receiving systems provide an SNR advantage over passive systems only in the cases where the system is device-noise limited, or when the receiver noise dominates. In this case, the noise generated by the NIC gets masked by the receiver's noise floor and does not affect the overall system NF. Furthermore, gain-enhanced passive antennas also have a much larger gain compared with non-Foster matched antennas, resulting in more sensitive systems that can detect lower signal levels. Therefore, non-Foster matched small antennas might not provide an actual performance advantage over gain-enhanced antennas in low-noise receiver systems.

Acknowledgment

The authors would like to thank J. Long for helpful discussions on antenna noise and for his assistance with measurements.

References

[1] H. A. Wheeler, "Fundamental limitations of small antennas," *Proc. IRE*, vol. 35, no. 12, pp. 1479–1484, Dec. 1947.

[2] L. J. Chu, "Physical limitations of omni-directional antennas," *J. Appl. Phys.*, vol. 19, no. 12, pp. 1163–1175, 1948. [Online]. Available: http://scitation.aip.org/content/aip/journal/jap/19/12/10.1063/1.1715038

[3] S. E. Sussman-Fort and R. M. Rudish, "Non-Foster impedance matching of electrically-small antennas," *IEEE Trans. Antennas Propag.*, vol. 57, no. 8, pp. 2230–2241, Aug. 2009.

[4] C. R. White, J. S. Colburn, and R. G. Nagele, "A non-Foster VHF monopole antenna," *IEEE Antennas Wireless Propag. Lett.*, vol. 11, pp. 584–587, Jun. 2012.

[5] M. M. Jacob, J. Long, and D. F. Sievenpiper, "Noise in non-Foster antenna matching circuits," in *Proc. IEEE Conf. Antennas Propag. Soc. Int. Symp. (APSURSI)*, Jul. 2013, pp. 2205–2206.

[6] C. Stedler, V. Wienstroer, and R. Kronberger, "Noise performance of an antenna matching network with negative-impedance converter (NIC)," in *Proc. 8th Eur. Conf. Antennas Propag. (EuCAP)*, 2014, pp. 2709–2713.

[7] J. G. Linvill, "Transistor negative-impedance converters," *Proc. IRE*, vol. 41, no. 6, pp. 725–729, 1953.

[8] *ANSYS HFSS*. accessed on 2014. [Online]. Available: http://www.ansys.com

[9] *Advanced Design System*. accessed on 2014. [Online]. Available: http://www.keysight.com

[10] D. F. Sievenpiper *et al.*, "Experimental validation of performance limits and design guidelines for small antennas," *IEEE Trans. Antennas Propag.*, vol. 60, no. 1, pp. 8–19, Jan. 2012.
[11] G. Skahill, R. Rudish, and J. Pierro. (2000). *Apparatus and Method for Broadband Matching of Electrically Small Antennas*. [Online]. Available: http://www.google.com/patents/US6121940
[12] C. A. Balanis, *Antenna Theory: Analysis and Design*, 4th ed. Hoboken, NJ, USA: Wiley, 2005.
[13] D. B. Sailors, "Techniques for estimating the effects of man-made radio noise on distributed military systems," in *Proc. Conf. Reduction Propag. Noise Effects Distrib. Military Syst. (AGARD)*, vol. 1. p. 14, 1990.
[14] *Characteristics and Applications of Atmospheric Radio Noise Data*, document 322-2, CCIR, International Radio Consultative Committee, International Telecommunication Union, Geneva, Switzerland, 1983.
[15] S. R. Best, "Realized noise figure of the general receiving antenna," *IEEE Antennas Wireless Propag. Lett.*, vol. 12, pp. 702–705, May 2013.
[16] P. R. Gray, P. J. Hurst, S. H. Lewis, and R. G. Meyer, *Analysis and Design of Analog Integrated Circuits*, 5th ed. Chichester, U.K.: Wiley, 2008.
[17] T. H. Lee, *The Design of CMOS Radio-Frequency Integrated Circuits*. Cambridge, U.K.: Cambridge Univ. Press, 2009.

Minu M. Jacob (S'11) received the B.S. degree in engineering from the Amrita School of Engineering, Coimbatore, India, in 2009. She is currently pursuing the Ph.D. degree with the University of California at San Diego, La Jolla, CA, USA.

Her current research interests include non-Foster circuits in broadband small antennas, active antenna applications, and microwave circuits.

Daniel F. Sievenpiper (M'94–SM'04–F'09) received the B.S. and Ph.D. degrees in electrical engineering from the University of California at Los Angeles, Los Angeles, CA, USA, in 1994 and 1999, respectively.

He was the Director of the Applied Electromagnetics Laboratory, HRL Laboratories, Malibu, CA, USA, where he was involved in artificial impedance surfaces, conformal antennas, tunable and wearable antennas, and beam steering methods. He is currently a Professor with the University of California at San Diego, La Jolla, CA, USA, where he is involved in antennas and electromagnetic structures. He has authored over 80 technical publications. He holds over 70 issued patents.

Dr. Sievenpiper received the URSI Issac Koga Gold Medal in 2008. He serves as the Chair of the IEEE Antennas and Propagation Society Committee on New Technology Directions. Since 2010, he has been serving as an Associate Editor of the *IEEE Antennas and Wireless Propagation Letters*.